Mechanism and Machine Theory 159 (2021) 104258

Contents lists available at ScienceDirect

Mechanism and Machine Theory

journal homepage: www.elsevier.com/locate/mechmachtheory

Kinematic comparison of single degree-of-freedom robotic gait trainers

Jeonghwan Lee[a], Lailu Li[b], Sung Yul Shin[c], Ashish D. Deshpande[a], James Sulzer[a,*]

[a] Department of Mechanical Engineering, University of Texas at Austin, 204 E Dean Keeton St, Austin, TX, 78712, USA
[b] Department of Intelligent Mechanical Systems Engineering, Kochi University of Technology, 185 Miyanokuchi, Tosayamada, Kami City, Kochi 782-8502, Japan
[c] Max Näder Lab for Rehabilitation Technologies and Outcomes Research, Shirley Ryan AbilityLab, Department of Physical Medicine and Rehabilitation, Northwestern University, 355 E. Erie St, Chicago, IL, 60611, USA

ARTICLE INFO

Article history:
Received 24 August 2020
Revised 14 January 2021
Accepted 14 January 2021

Keywords:
Dimensional synthesis
Affordable technology
Electromechanical gait training
Physical therapy

ABSTRACT

Single degree-of-freedom mechanized gait trainers employing linkage mechanisms can imitate the gait trajectory of the human user at a potentially lower cost than current commercial solutions. Our goal was to evaluate recently introduced four-, six- and eight-bar designs from the standpoint of kinematics, that is, the ability to follow a natural gait pattern. Based on a gait database of 113 healthy individuals, we synthesized mechanisms allowing two link length adjustments and compared trajectory and path accuracy of the ankle position across mechanisms. We used cross-validation to obtain data-independent accuracy measures. We used gait trajectories from a large human database and predicted additional trajectories to represent the effects of varying heights and speeds. We found that trajectory error was significantly lower in the eight-bar mechanism (3.76 ± 0.18 cm, mean ± SD) than the four- (6.84 ± 0.37 cm) and six-bar (7.15 ± 0.48 cm) configurations ($p < 0.0001$). However, we did not observe differences in time-independent path error between configurations or in mechanical advantage ($p > 0.05$). We conclude that the optimized eight-bar configuration is best when the mechanism is tied to a constant velocity actuator, whereas the optimized four-bar mechanism performs as well if the actuator is well-controlled.

1. Introduction

Gait impairments, including reduced gait speed and stride length, abnormal gait kinematics and kinetics, and asymmetry step length, are common among those with neurological insults such as stroke or spinal cord injury [1,2]. These issues arise due to weakness [3], spasticity [4], and discoordination [5,6] among other impairments. It is critical to have as much training as possible within the first months following injury [1,7], yet patients often transfer to lower-intensity outpatient therapy programs within weeks due to healthcare coverage restrictions [8]. Robot-assisted gait training has been proposed as a potential solution to increase patient throughput with intensive, repetitive, and task-oriented motor activities [9,10]. These trainers, such as the Lokomat (commercially available from Hocoma AG, Volketswil, Switzerland) [11], are often composed of

* Corresponding author.
E-mail addresses: jlee85@utexas.edu (J. Lee), 248008f@gs.kochi-tech.ac.jp (L. Li), sshin@ricres.org (S.Y. Shin), ashish@austin.utexas.edu (A.D. Deshpande), james.sulzer@austin.utexas.edu (J. Sulzer).

https://doi.org/10.1016/j.mechmachtheory.2021.104258
0094-114X/

four actuators (or more) to actively control knee, hip (and pelvic) motion during walking [12]. However, the high capital cost of these trainers makes them inaccessible to the vast majority of in/outpatient clinics. While robotic gait training exhibits similar or better clinical benefits compared to conventional therapy [13,14], the high capital cost could negate the ostensible financial labor-saving benefit of robotic training.

Cost reduction could be achieved through clever design features. Since most commercialized robotic trainers use a single fixed trajectory focused on sagittal plane gait motion, a multiple degrees-of-freedom (DOFs) robotic gait trainer may not be necessary. Therefore, simpler designs with 1 DOF linkage mechanisms have been introduced. The Gait Trainer (GT I) is an early example of robotic locomotor training using a single motor [15,16], now in its commercialized iteration (GT II). Based on a double crank and rocker gear system, the GT I/GT II is an elliptical trainer that drives end effector (foot) position, with some evidence of clinical success in stroke survivors [17]. Yet the elliptical designs do not produce accurate gait trajectories nor provide cutaneous stimulation of ground contact experienced during walking, potentially critical components to gait recovery [18].

In addition to ground contact, our main goals for a 1 DOF gait trainer were accurate reproduction of a human-like gait pattern and the ability to adapt to individuals. Advanced mechanism synthesis methodology can be used to achieve these goals. Approximate synthesis using numerical methods has been applied to a linkage mechanism design based on actual human gait data. Ji et al. optimized a four-bar with normative ankle trajectory by solving a nonlinear least-square problem [19], and Kora et al. optimized it by a trust region-reflective algorithm [20]. Tsuge et al. applied a hopotomy directed optimization for a Stephenson III six-bar and a ten-bar synthesis based on a single subject's ankle trajectory [21–23]. Shao et al. employed a genetic algorithm to design a cam-linkage mechanism based on Stephenson III six-bar with ankle trajectory from normative gait data [24]. Our own group recently introduced an eight-bar design based on a gait database of 113 healthy individuals [25]. The optimization problem for linkage synthesis was solved by the interior point method. We found that with a crank at a constant speed, an eight-bar design was capable of accurately facilitating gait motion over a wide range of human gait patterns with an offline adjustment of only two link lengths. Subsequent work by other researchers has further investigated this design with a single participant's ankle trajectory by a model-independent method based on the optimal trajectory tracking control of a shadow robot [26,27]. However, a follow-up question has not been addressed: are simpler designs such as four- or six-bar mechanisms capable of exhibiting comparable performance? Simpler designs might be preferable because of the potential for further cost-savings and ease of operation and maintenance. A preliminary analysis in our previous work suggested that an eight-bar design has greater trajectory accuracy than a four-bar design operating at constant crank velocity [25]. However, this initial analysis did not address differences in gait speed, height, or a device capable of changing the crank velocity. A controlled crank velocity would be more amenable to situations of variable-speed overground training, whereas a constant velocity would be more appropriate for typical constant-speed treadmill training scenarios.

The objective of this study was to investigate three different 1 DOF linkage mechanisms that have been previously proposed in gait trainers: a four-bar [20], a Stephenson III six-bar [22], and an eight-bar mechanism [25]. The primary question of this study was to compare the kinematic accuracy of these mechanisms and determine their relative benefits. We based our analysis on a gait dataset of 113 healthy human individuals [28] and used regression models to synthesize predicted changes in gait with height and speed [29]. We extracted the end effector (i.e., ankle position) error, both the time-dependent trajectory error and the time-independent path error, corresponding to constant input velocity and variable input velocity operation, respectively. We employed cross-validation to eliminate data bias and systematically investigated kinematic accuracy variation affected by varying height and gait speed. In addition to end effector kinematics, we computed the mechanical advantage of the mechanism to identify the efficiency in force transfer of each design. This work presents a novel basis for objective comparison and insight into 1 DOF gait trainer designs. These insights will help prescribe the most appropriate mechanism for economical and accessible robotic gait training aimed at moderately to severely neurologically impaired individuals.

2. Dimensional synthesis

This study focuses on three different mechanisms: four-, six-, and eight-bar configurations offered in previous work [20,22,25]. The canonical topologies of these designs are illustrated in Fig. 1. The linkage design for the 1 DOF gait trainer should have the capability of gait pattern reproduction, and it should be easily customizable to individuals. The following section details the dimensional synthesis to human gait data to obtain a best-fit customizable linkage configuration.

2.1. Prescribed Canonical Gait Patterns

Dimensional synthesis is an inverse problem that obtains the linkage dimensions required to achieve a prescribed output motion. To establish generality, we used multiple prescribed output motions (gait trajectories) representing the large variability of human gait [30]. Each gait trajectory was reflected as the time-dependent motion of the lateral malleolus. We reconstructed a total of nine canonical prescribed human gait trajectories from a database of 113 healthy individuals (50 male / 63 female, age 44.27 $\pm$ 14.93, height 164.82 $\pm$ 8.32 cm) walking at 3.0 km/h on a treadmill [28]. The nine prescribed gait trajectories consisted of the grand mean (*meta)*, largest, smallest, as well as six intermediate motions linearly interpolated from the former three (Fig. 2) by the profile blending method [31] to more thoroughly span the manifold. The largest

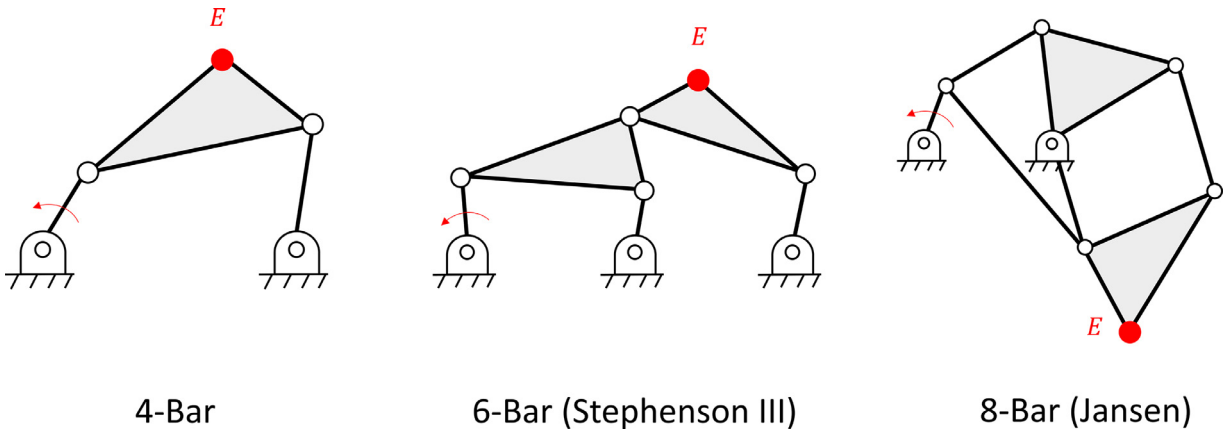

Fig. 1. Linkage mechanism structural representation: four-bar, six-bar (Stephenson III), and eight-bar (Jansen) mechanisms. The designated end effector for gait pattern generation is denoted by *E*.

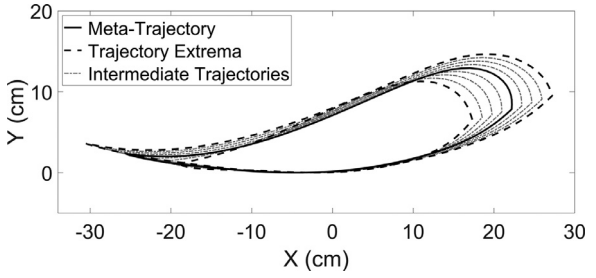

Fig. 2. A total of nine reproduced reference natural human gait motions of the ankle joint (e.g., lateral malleolus) from the gait kinematic database. The mean of all subjects' gait motions is called the meta-trajectory (solid line). The largest and smallest gait trajectory (dashed lines) and interpolated gait trajectories (dotted lines) are in the Cartesian frame.

and smallest trajectories were an average of selected groups of 10 individuals with the largest and smallest step lengths (upper and lower quantile of the database, respectively). We extracted the ankle trajectory relative to the hip in the sagittal plane divided into the single gait cycles based on heel strike events. All single gait cycle trajectories were normalized into 100-time frames. The reference gait trajectory, T_{ref}, is defined by $\{\mathbf{x}_{ref,\ i} \in \mathrm{R}^2 :\ \forall i \in \{1, \cdots, N\}\}$ where $\mathbf{x}_{ref,i}$ is a position vector of human ankle for the i-th time instance and N is the total number of time frames.

2.2. Optimization

The goal of optimization was to find the optimal linkage parameters that minimize the kinematic error with respect to human reference gait motion. Here, we established a multi-objective function towards minimizing spatial and temporal motion differences between a machine and a human. Then, we introduced an iterative optimization scheme to determine the optimal adjustable link selection for customizing the device's trajectory to a wide range of gait patterns.

2.2.1. Objective Functions

The first objective function was mainly based on a prescribed reference gait trajectory, T_{ref}, determined in Section 2.1 and a trajectory of the mechanism end effector, T_E. The mechanism's output trajectory is defined as $\{\mathbf{x}_{E,i} \in \mathbb{R}^2 :\ \mathbf{x}_{E,i} = f(\theta_{c,i},\ \boldsymbol{Z}),\ \forall i \in \{1, \cdots, N\}$ and $\theta_{c,i} = \frac{2\pi}{N}(i-1) \in [0,\ 2\pi]\}$, where $\mathbf{x}_E$ is a position vector of the end effector computed by a well-known analytical kinematic approach, the vector loop method [32]. The analytical kinematics is simplified as the function of the input crank angle, θ_c, and a vector of linkage parameters, $\boldsymbol{Z} = [l_1,\ l_2,\ \cdots, l_a,\ \alpha,\ \emptyset_1, \cdots,\ \emptyset_b]$ where l is a link length, α is an angle of a ternary link if existing, $\emptyset$ is an angle of a ground link, for the mechanisms shown in Fig. 1. Here, θ_c was equally distributed for one revolution by N samples, representing constant crank velocity. The objective function, J_1, is the root mean square (RMS) error between T_{ref} and T_E, formulated as

$$J_1(\boldsymbol{Z}) = \sqrt{\frac{1}{N}\sum_{i=1}^{N}\left\|\mathbf{x}_{ref,i} - \mathbf{x}_{E,i}(\boldsymbol{Z})\right\|^2}. \tag{1}$$

The objective function is based on a prescribed human-like trajectory [20,25]. However, a geometrical shape in a motion could not be ideally matched by such a structural error function since it limits the search space [33]. In order to expand

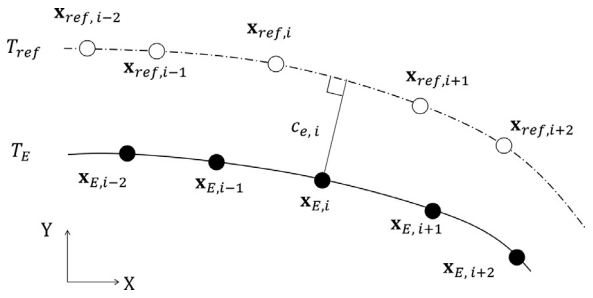

Fig. 3. The contour error, c_e, which is the shortest orthogonal distance between the desired human reference and the generated machine trajectory.

a search space and match a shape in a motion simultaneously, contour error between trajectories was used as the second objective. As shown in Fig. 3, the contour error, c_e, is the shortest orthogonal distance between the desired human reference and the generated machine trajectory. The contour error provides a better shape indicator than the structural error due to its flexibility in timing. We deployed the local circular approximation [34] to estimate the contour error. The objective function, J_2, represents an overall contour error between trajectories formulated as

$$J_2(\boldsymbol{Z}) = \sqrt{\frac{1}{N}\sum_{i=1}^{N} c_{e,i}(\boldsymbol{Z})^2}. \tag{2}$$

We solved this two-objective problem by the ε-constraint method [35], which is applicable for the non-convex nonlinear problem. In the ε-constraint method, we minimize the objective function J_2 using J_1 as constraints, incorporating them in the constraint part of the model as shown below.

$$\begin{aligned} \textbf{minimize} \quad & J_2(\boldsymbol{Z}) \\ \textbf{s.t.} \quad & J_1(\boldsymbol{Z}) \le \varepsilon_1 \\ & J_1(\boldsymbol{Z}) \le J_2(\boldsymbol{Z}) \\ & l_1 + l_2 - l_3 - l_4 \le 0 \\ & FC_{max}\left(T_{ref}\right) = FC_{max}(T_E) \\ & \boldsymbol{Z}_{LB} \le \boldsymbol{Z} \le \boldsymbol{Z}_{UB} \end{aligned} \tag{3}$$

The ε-constraint method can obtain different optima in the Pareto front by a systematic variation of the constraint bound, ε_1 [36]. The ε-constraint method needs attention in the selection of the bound since it should lie in the feasible objective space to acquire the proper solutions. Because we empirically identified the feasible objective space of J_1, we set ε_1 as 15 cm, which is between the minimum and maximum cost of J_1 across all mechanisms. This allows us to guarantee for a non-dominant solution weighted more on shape within our model. Additionally, since we know the cost of J_2 is always larger than J_1, we limited the search space satisfying $J_1 \le J_2$ for the efficiency in search. In order to guarantee the input crank rotates continuously, we set another inequality constraint using Grashof's condition [32] for the four-bar linkage loops in which the input crank is involved inside each mechanism ($l_1 l_2 l_3 l_4$ loop of the four- and the six-bar; $l_1 l_2 l_3 l_4$ and $l_1 l_7 l_8 l_4$ loops of the eight-bar in Fig. 5). We also constrained a solution to have the same maximum foot clearance between trajectories. FC_{max} denotes the function of maximum foot clearance computing the difference between the maximum and minimum y-axis values of position vectors in a trajectory. This allows the solution to avoid an abnormal shape (e.g. flattened). Lastly, $\boldsymbol{Z}_{LB}$ and $\boldsymbol{Z}_{UB}$ are lower and upper bounds of a linkage parameter vector, respectively. Lower bounds for link length parameters were zero, which means searching only positive values, and there were no upper bounds. For angular parameters, there were no upper or lower bounds. Variable and fixed linkage configurations were differently organized depending on the purpose of optimization described in the following sections.

2.3. Customizing The Trajectory With Limited Adjustments

The individual link lengths of the mechanisms can be adjusted to fit a wide array of gait trajectories. However, it is time-consuming and impractical to adjust every link of a given mechanism, especially in a clinical setting. Based on our earlier research and input from our clinical partners, we determined an offline adjustment of two links as a practical limit for clinical use [25]. Thus, to be consistent across mechanisms, we limited our synthesis to have only two link adjustments of any link except for the input crank length. The following procedure describes an iterative optimization scheme to determine the optimal two adjustable link combination.

The iterative optimization procedure was initiated from three different initial linkage parameter vectors attempting to scan the global minima. We performed pre-optimization to specify three initials by the following steps:

1) Specify the base initial linkage parameter vector, $\boldsymbol{Z}_{base} = [l_1,\ l_2,\ \cdots, l_a,\ \alpha,\ \emptyset_1, \cdots,\ \emptyset_b]$

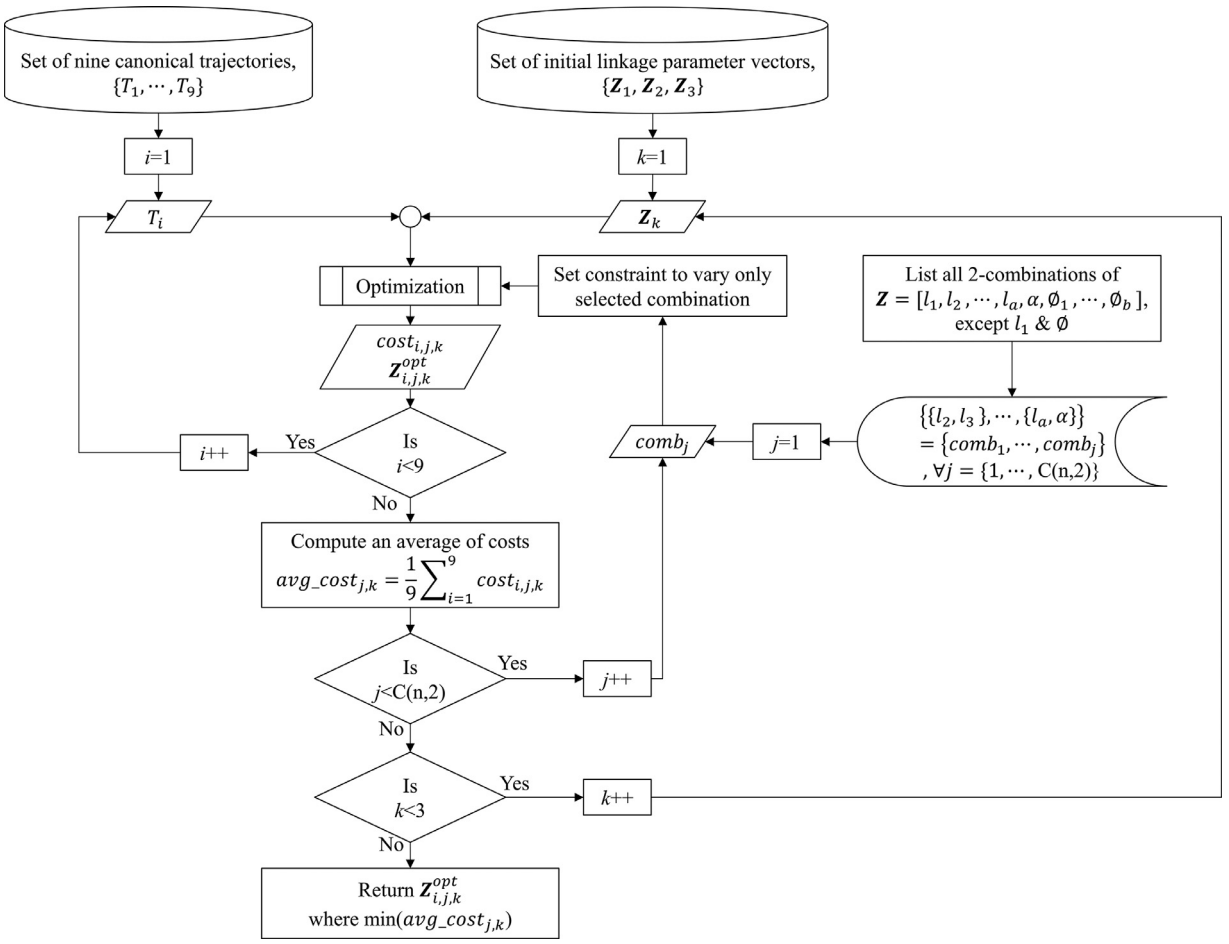

Fig. 4. Flowchart for an iterative optimization procedure to determine the optimal linkage configuration, including two-adjustable link combinations.

2) Optimize $\boldsymbol{Z}_{base}$ for the meta-trajectory and two extrema trajectories (Fig. 2), respectively, by varying all parameters.
3) Return the solutions as a set of initials $\{\boldsymbol{Z}_1, \boldsymbol{Z}_2, \boldsymbol{Z}_3\}$.

For $\boldsymbol{Z}_{base}$ in Step 1, we deployed the dimensions reported by the representative papers of each mechanism [20,22,25]. Based on three initials acquired in Step 3, we iteratively optimized the mechanism for a set of nine canonical trajectories (Fig. 2) and scrutinized the best two-adjustable links combination as shown Fig. 4.

Fig. 5 and Table S1 represent an optimized linkage configuration and parameters through the iterative optimization procedure. The blue labeled links are the adjustable links to produce an individual-specific gait trajectory. In practice, the one-time optimization using the same objective function in Section 2.2.1 must be performed to compute the lengths of the adjustable links for the new individual trajectory while maintaining the other link parameters fixed. The new individual trajectory will be the predictive target gait trajectory. This can be acquired by the regression model [29] or stochastic prediction algorithm [28] based on patients' anthropometric and experimental data. The whole process was implemented in MATLAB R2019b (Mathworks Inc., Natick, MA) by using the *fmincon* function. We employed a sequential quadratic programming (SQP) method [37] as a nonlinear problem solver.

3. Evaluation

The primary aim of this study was to evaluate the output kinematics of a synthesized mechanism based on human gait motion and determine the optimal design among selected 1 DOF mechanisms. We conducted two evaluation processes. First, we compared mechanisms based on walking data of 113 healthy human individuals [28], followed by cross-validation to correct for biasing (Section 2.1). Second, we compared the effects of height and gait speed on kinematic accuracy between mechanisms via a set of 100 simulated gait trajectories.

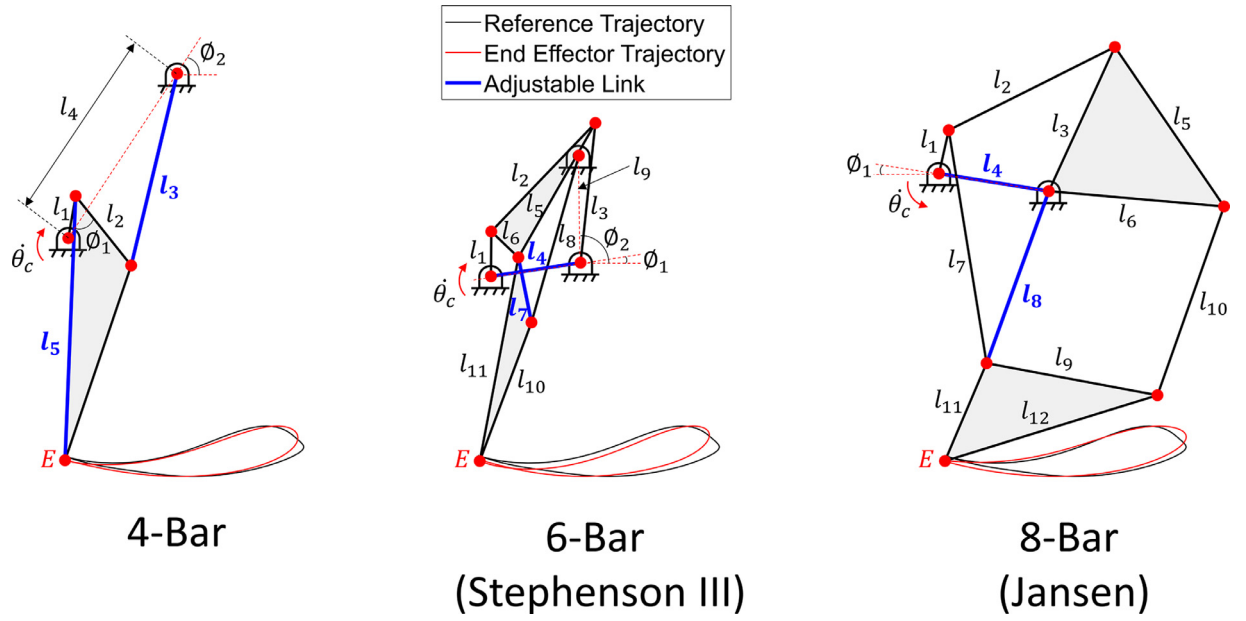

Fig. 5. Optimized linkage configuration and optimization parameters. Blue colored links are adjustable links required to be changed offline to create individualized gait patterns. Other link parameters are fixed after synthesis.

3.1. Outcome Measures

The primary focus of this study was the kinematic accuracy of the end effector compared to the measured human ankle position during treadmill walking. We examined the kinematic accuracy both as a function of time (trajectory error via constant crank velocity) and independent of time (path error). We used the costs of each objective function (J_1 and J_2 in Section 2.2.1) as these outcome measures. J_1 represents the trajectory error which is the RMS distance between the end effector and ankle positions at given time points. J_2, the RMS contour error, indicates the path error which is a time-independent geometric shape difference. Simultaneously, we extracted the respective peak errors.

While we expected to see differences in kinematic error between configurations, we additionally wanted insight into the effort required to traverse these paths. Thus, we computed a mechanical advantage, M_A, of each mechanism. M_A is an applied force ratio between input and output, known as the force amplification. Given the conservation of energy, the ideal mechanical advantage can be rewritten by the relationship of the linear velocity as follows,

$$M_A = \frac{F_{out}}{F_{in}} = \frac{\tau_{out}}{r_{out}} \cdot \frac{r_{in}}{\tau_{in}} = \frac{\omega_{in}}{\omega_{out}} \cdot \frac{r_{in}}{r_{out}} = \frac{v_{in}}{v_{out}}, \tag{4}$$

where F is force, τ is torque, r is the moment arm, ω is the angular velocity of a rigid body, and v is the linear velocity. In this study, we specified the input velocity, v_{in}, as the linear velocity at the distal joint of input crank from the ground. To compute v_{in}, we used the constant 2π rad/s for ω_{in} to match the given walking speed, and employed the optimized input crank length (l_1 in Fig. 5) for r_{in}. The linear velocity, which is tangential to the trajectory of the end effector (E in Fig. 5), was set as the output velocity, v_{out}. This can be calculated by the numerical derivative of the end effector trajectory. We then extracted a portion of force amplification ($M_A > 1$) during one gait cycle as a secondary outcome measure to determine the efficiency in terms of force transfer.

3.2. Cross-Validation

The canonical prescribed gait patterns in Section 2.1 could be biased if based on a small sample. In order to conduct an unbiased and generalized comparison, we employed cross-validation [38,39] over the entire gait database. Under cross-validation, the available data are divided into k disjoint sets, called a fold. The k models are then trained, each on a different combination of $k - 1$ partitions, and tested on the remaining partition. The k-fold cross-validation estimate is the mean for each of the k models over the corresponding test partitions of the data. In this study, we used 10-fold cross-validation. We equally but randomly distributed the gait trajectories into folds from our database of 113 individuals at the stage of creating prescribed human trajectories in Section 2.1. After data distribution, each fold contained ten individual gait trajectories; therefore, the training set had 90 individuals' ($k - 1$ folds of total) and the test set had ten individuals' gait trajectories. As a result, every iteration in the cross-validation returned different sets of nine canonical trajectories and resulted in ten dif-

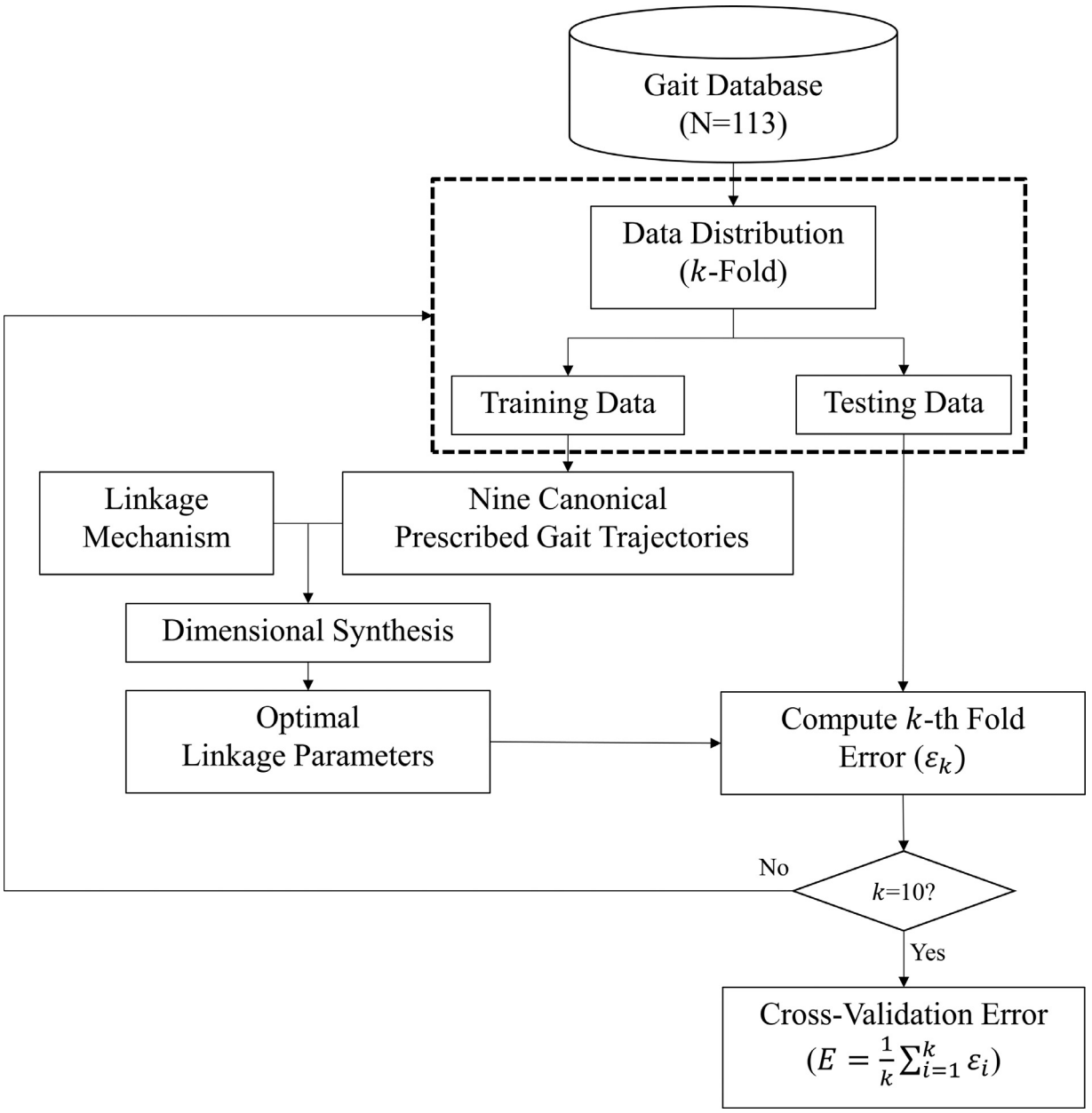

Fig. 6. Evaluation flowchart for 10-fold cross-validation. Data distribution was conducted at the stage of reference trajectory generation. Cross-validation error is an average of all 10 folds of error.

ferent optimal configurations by the proposed dimensional synthesis. Then, we cross-validated results for the corresponding testing data. The flowchart of our 10-fold cross-validation procedure is represented in Fig. 6.

3.3. Effects Of Height And Gait Speed On Kinematic Accuracy

We evaluated the ability to match across a range of gait trajectories with varying heights and walking speeds. We generated an independent set of 100 gait trajectories based on previously determined algorithms of how gait trajectories change with height and speed [29]. This algorithm provided time-normalized joint trajectories (hip flexion/extension, abduction/adduction, knee flexion/extension, and ankle dorsiflexion/plantar flexion) with the input of arbitrary walking speed and an individual's height. We set our target range of the walking speed between 0.5 and 5 km/h with 0.5 intervals, and the height ranging from 152 to 188 cm with 4 cm intervals. We then extracted the joint trajectories of 10 discrete walking speeds for each of 10 discrete heights. The ankle trajectories in the sagittal plane were calculated by imposing the joint

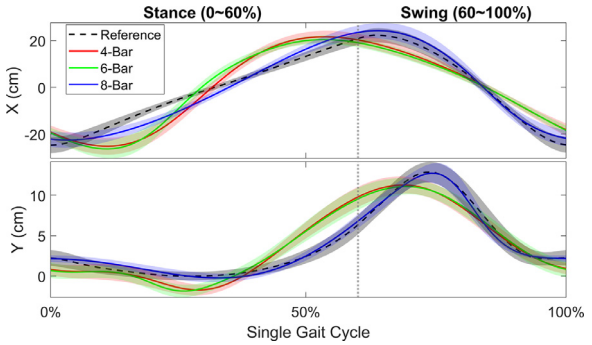

Fig. 7. Average trajectory of all tested individuals by the cross-validation (dashed black) compared to four-bar (red), six-bar (green) and eight-bar (blue) configurations in anterior-posterior (X) and superior-inferior (Y) directions. The shaded area represents the standard deviation.

Table 1
Cross-validation errors: Mean and standard deviation of trajectory and path errors (RMS and peak error) for each mechanism configuration across cross-validation folds.

		4 bar	6 bar	8 bar
Trajectory Error (J_1)	RMS (cm)	6.84 ± 0.37	7.15 ± 0.48	3.76 ± 0.18
	Peak (cm)	11.42 ± 0.51	11.70 ± 0.71	7.80 ± 0.33
Path Error (J_2)	RMS (cm)	0.65 ± 0.12	0.67 ± 0.17	0.63 ± 0.09
	Peak (cm)	1.27 ± 0.18	1.28 ± 0.26	1.41 ± 0.17

trajectories to the lower body kinematic model developed with lower limb lengths estimated by height [40]. As a linkage configuration to be tested, we employed the linkage solution from the 10-fold cross-validation (Section 3.2) that had shown the minimum error and variance for both trajectory and path errors among k folds. The selected linkage configuration, including two adjustable links, was optimized for the aforementioned 100 gait trajectories by optimizing only two adjustable links.

3.4. Statistics

We used a linear mixed model [41] for the statistical comparison of cross-validation errors across the mechanisms. The dependent variable was the trajectory or path error, with a fixed variable of the type of mechanism and a random effect of fold coefficients. Tukey *post hoc* t-tests were used to compare pairwise conditions.

4. Results

4.1. Effect Of Configuration On Kinematic Accuracy Based On Gait Database

The generalized kinematic accuracy across 113 individuals and the relative performance between mechanisms were determined based on the cross-validation in Section 3.2. The differences in how the trajectory error between mechanisms changes over the gait cycle can be illustrated with the timecourse of the ankle position. Fig. 7 is based on an average of all tested individuals' ankle trajectories in the anterior-posterior (X) and superior-inferior (Y) directions (dashed black). The eight-bar trajectory in both directions (blue) matches very closely with the reference trajectory. However, the four-bar (red) and six-bar (green) show less agreement with the reference trajectory and more agreement with each other.

These effects carried into the larger comparison across all individuals. We found a significant difference in trajectory RMS error between mechanisms ($F(2, 288) = 354.07$, $p < 0.0001$). At the pairwise level, we observed a significant decrease in trajectory RMS error of the eight-bar compared to the four-bar (mean difference = 3.07 cm, $t(288) = 21.87$, $p < 0.0001$) and six-bar (mean difference = 3.38 cm, $t(288) = 24.07$, $p < 0.0001$). There was no statistically significant difference in trajectory RMS error of the four-bar compared to the six-bar configuration (mean difference = -0.31 cm, $t(288) = -2.20$, $p = 0.09$). We found the same relations with peak trajectory error ($F(2, 288) = 183.48$, $p < 0.0001$). The peak trajectory error in the eight-bar configuration was significantly less than in the four-bar (mean difference = 3.61 cm, $t(288) = 15.91$, $p < 0.0001$) and in the six-bar (mean difference = 3.90 cm, $t(288) = 17.20$, $p < 0.0001$) configurations. We did not observe significant difference in the peak trajectory error of the four-bar configuration compared to the six-bar configuration (mean difference = -0.29 cm, $t(288) = -1.29$, $p = 0.60$). Results are summarized in Table 1. As a basis for comparison, we extracted the within-subject variance of the ankle trajectory from our gait data at 5.02 cm. This is substantially more than the eight-bar trajectory error (3.76 cm), but less than the four- and six-bar trajectory error (6.84 and 7.15 cm, respectively).

We did not observe differences in path error among mechanism configurations. We compared path RMS error ($F(2, 288) = 0.58$, $p = 0.56$) as well as path peak error ($F(2, 288) = 1.29$, $p = 0.28$). All results are presented in Table 1. The

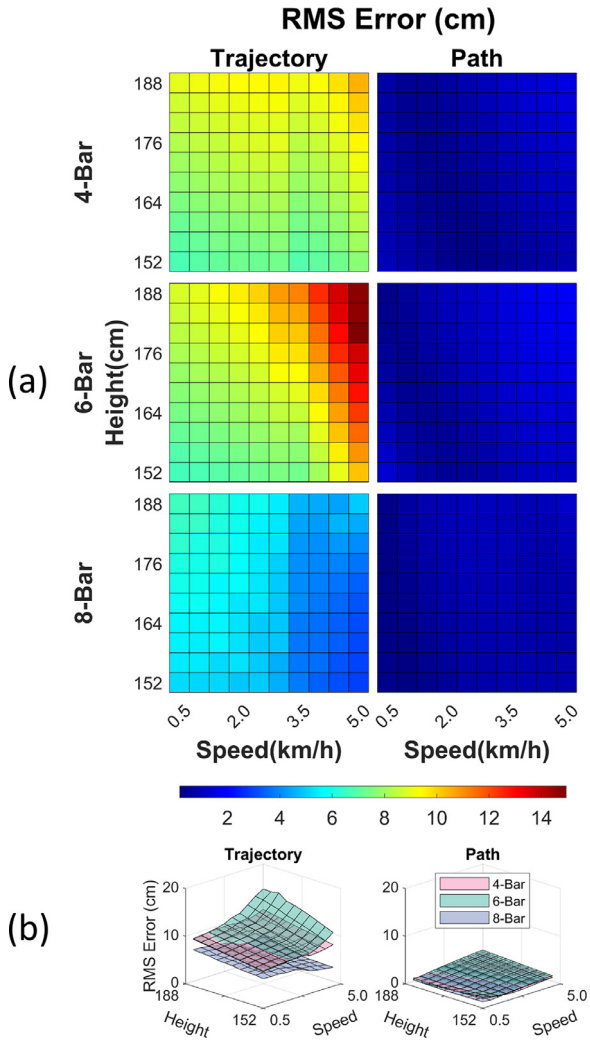

Fig. 8. The heat map (a) and the surface plot (b) for the trajectory (left) and the path (right) RMS error across gait patterns varied by height and walking speed.

Table 2
Mean and standard deviation of trajectory and path errors (RMS and peak error) for each mechanism configuration across varying heights and speeds.

		4 bar	6 bar	8 bar
Trajectory Error (J_1)	RMS (cm)	8.31 ± 0.79	9.38 ± 1.97	4.84 ± 0.99
	Peak (cm)	14.28 ± 1.57	16.68 ± 4.87	10.30 ± 2.02
Path Error (J_2)	RMS (cm)	0.74 ± 0.33	1.02 ± 0.43	0.71 ± 0.26
	Peak (cm)	1.51 ± 0.58	2.22 ± 1.04	1.33 ± 0.62

within-subject variance of the ankle path was 3.83 cm, far above the path errors of the mechanism configurations of 0.63 ~ 0.67 cm.

4.2. Effects Of Heights And Gait Speed On Kinematic Accuracy

The effect of height and gait speed on kinematic accuracy provides additional insight. A comparison of trajectory and path RMS error are presented as heat maps and 3D surface plots in Figs. 8a and b, respectively. Peak errors are illustrated in Fig S1. A summary of the results is shown in Table 2. Across all gait patterns, the eight-bar mechanism had the lowest average trajectory RMS error (4.84 cm), with higher average trajectory error in the six-bar (9.38 cm) and four-bar (8.31 cm) mechanisms. We observed the same relations for peak trajectory error, albeit with higher magnitudes (Table 2). The eight-

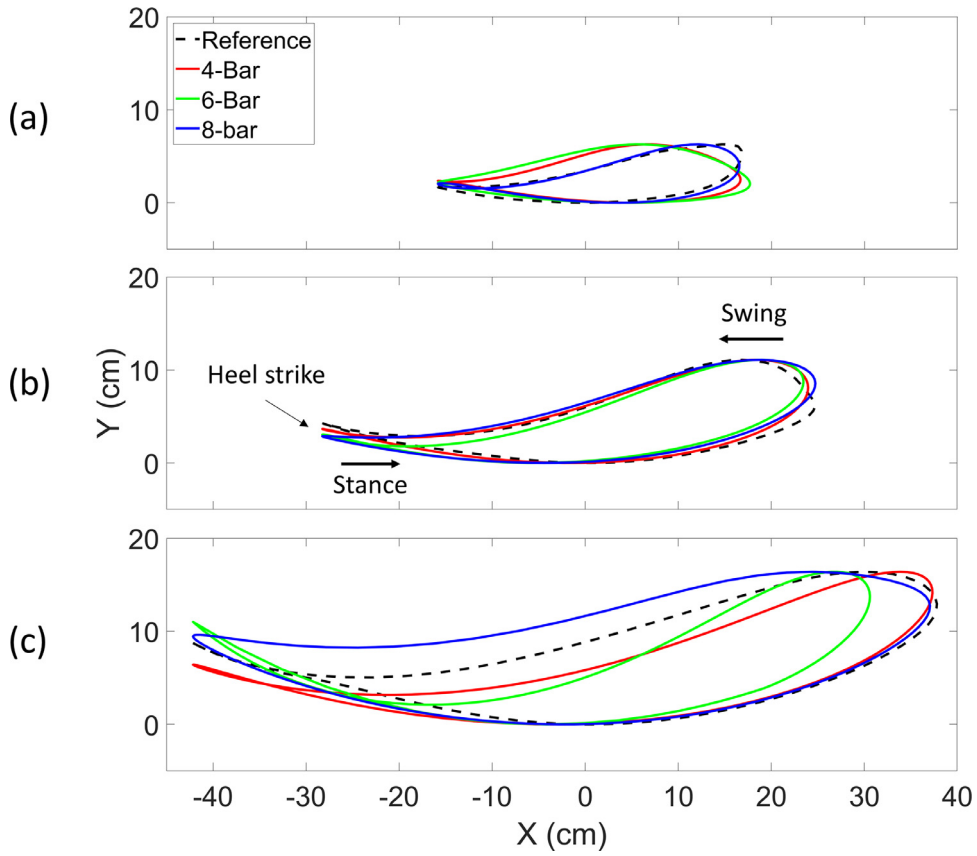

Fig. 9. Paths of three representative cases (dashed black) compared to four-bar (red), six-bar (green) and eight-bar (blue) configurations in sagittal plane (X-Y): (a) the smallest case (0.5 km/h gait speed, 152 cm height), (b) the median case (2.5 km/h gait speed, 168 cm height), and (c) the largest case (5.0 km/h gait speed, 188 cm height).

bar mechanism exhibited similar variance to the four-bar mechanism (0.99 and 0.79 cm, respectively) throughout the space, both lower than the six-bar mechanism (1.97 cm). The trajectory RMS and peak error of the four-bar mechanism performed best at small heights and low gait speeds and worst at large heights and high gait speeds (Fig. 8a, left top). We observed the same relations with the six-bar mechanism but with greater variance (Fig. 8a, left middle). The eight-bar mechanism exhibited its best trajectory RMS error performance at small heights and high gait speeds, and its worst performance at large height and low gait speeds (Fig. 8a, left bottom).

Compared to trajectory error, there was a prominent decrease in path error across all mechanisms. All mechanisms similarly exhibited path errors below a centimeter. Specifically, the four-bar and the eight-bar mechanisms exhibited similar path RMS error and variance (0.74 $\pm$ 0.33 cm and 0.71 $\pm$ 0.26 cm, respectively), both lower than the six-bar mechanism (1.02 $\pm$ 0.43 cm, Table 2). Peak path errors mirrored these relations (Table 2). The performance of the mechanisms can be directly compared in the overlaid 3D surface plots in Fig. 8b.

Although all mechanisms showed an accurate path RMS error, there were notable outliers at extrema gait speeds. Fig. 9 illustrates synthesized paths in the sagittal plane (X-Y) from three representative cases based on gait motion size. The eight-bar path (blue) matched very closely with the reference path at the lowest gait speed of 0.5 km/h and the smallest body height of 152 cm (Fig. 9a). However, the four-bar (red) and six-bar (green) show less agreement with the reference path and more agreement with each other. Such an abnormal path in the four-bar and the six-bar mechanisms was observed only at the lowest gait speed of 0.5 km/h but reduced as height increased above 160 cm. At the highest gait speed of 5.0 km/h and the largest body height of 188 cm (Fig. 9c), we observed a relatively larger distortion of the path in the six-bar mechanism than in the four-bar and the eight-bar mechanisms. We often observed the same unnatural paths at higher gait speeds ($>$3.0 km/h) and larger heights ($>$172 cm) accompanying larger trajectory errors. On the other hand, the four-bar and the eight-bar configuration mostly showed a well-matched path with the reference having about the same step length and foot clearance at higher gait speed. However, both mechanisms exhibited larger path deviations during the swing phase compared to the synthesized path at the median range of gait speed.

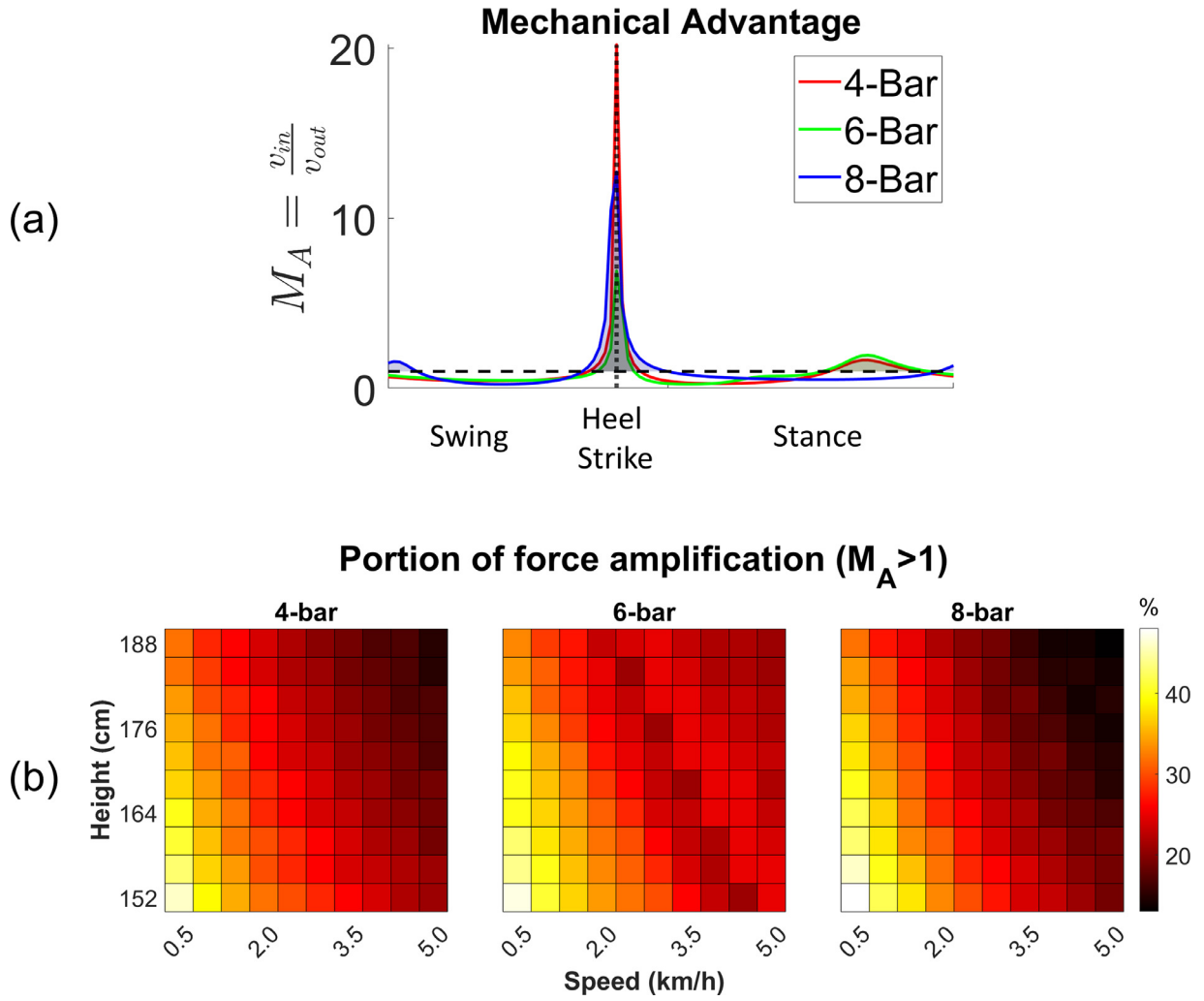

Fig. 10. a) Time course of mechanical advantage for three mechanism configurations. Peak mechanical advantage occurs at heel strike in all cases. b) Heat map for the portion of force amplification where $M_A > 1$ across gait patterns varied by height and walking speed. The shaded area in an example mechanical advantage plot indicates where the input force is amplified. Maximum mechanical advantage occurs at heel strike event.

4.3. Force Amplification

We did not observe a substantial difference between mechanism configurations in force amplification. Fig. 10a shows the time course of mechanical advantage for the case at 2.5 km/h gait speed and 172 cm height. In this case, approximately 25% of the gait cycle in each case resulted in a mechanical advantage above 1. Across varying speeds and heights, greater mechanical advantage (percentage of gait cycle with M_A>1) overall was observed at small heights and low gait speeds (Fig. 10b). This contrasted with less mechanical advantage at large heights and high gait speeds. The smallest portions of the gait cycle showing force amplifications across configurations were 15% of the gait cycle in the four-bar, 21% in the six-bar, and 14% in the eight-bar configurations. Across all gait patterns, the peak mechanical advantage was typically observed at the heel strike event (Fig. 10a).

5. Discussion

In this work, we investigated the performance of three candidate mechanisms, four-, six- and eight-bar configurations, previously presented as solutions for electromechanical gait training [20,22,25]. We evaluated these mechanisms in terms of their kinematic accuracy in comparison to a large dataset of healthy individuals' gait trajectories using an optimization algorithm that adjusted two link lengths. We additionally reported kinematic error propagation of these mechanisms across different gait patterns based on varying height and walking speed. In the condition of a constant crank velocity, we observed that the eight-bar mechanism had less kinematic error than the four- and six-bar configurations between individuals or

across heights and gait speeds. However, the time-independent path error between configurations was nearly identical. This work represents the first systematic comparison of single degree-of-freedom robotic gait trainer designs. These data provide a nuanced picture of which conditions are ideal for different mechanism configurations, resulting in a more effective situational design of mechanized gait trainers. These simplified gait trainers may be ideal as a more financially accessible electromechanical gait training option for clinics and at home.

The primary finding is that at constant crank velocity, the eight-bar mechanism has the lowest kinematic error of the three designs. Situations where constant crank velocity may be preferred include treadmill walking, especially if the machine itself is driven by the treadmill motor, similar to earlier versions of the LokoHelp [42]. Anchoring the input of the trainer to the treadmill negates the need for control, potentially reduces cost, and improves stability. The eight-bar was also the only configuration with an error under the within-subject gait trajectory variance, suggesting the clinical significance of the performance. The reduction in error relative to other mechanisms was invariant to different gait patterns derived from simulated changes in height and walking speed. The primacy of the eight-bar mechanism was expected since it has the greatest number of links, and thus has the greatest optimization flexibility for a desired gait pattern. This finding agrees with and extends our previous limited analysis comparing the eight-bar to a four-bar mechanism [25].

However, for cases where the mechanism is driven by its own motor independently, for example, in an overground walking configuration [20,43], our results are not as clear. Based on the time-independent path error, we found the roughly equivalent performance of all three mechanism configurations. The errors were roughly equally low both compared to a large human gait dataset and gait patterns with simulated changes in height and gait speed. We expected to find that the eight-bar mechanism would perform better than the other two mechanisms. Instead, we observed that the kinematic tracking error of these mechanisms is governed by temporal instead of spatial considerations. We conclude that a greater number of links alone does not guarantee improved spatiotemporal behavior. Thus, based solely on kinematic error, given a well-controlled crank velocity, the four-bar mechanism [19,20] is likely the best solution of the three configurations due to its simplicity.

One of the innovations of this work is that we compared the three mechanism configuration kinematics to a large human gait database [28] and simulated gait patterns with various heights and walking speeds [29] for a more comprehensive benchmark. Anthropometric parameters and walking speed modulate gait patterns [30,44]. However, this large variance of gait patterns across individuals and walking speeds has been disregarded in most gait trainer design studies using 1 DOF planar linkage mechanisms. Commonly a single gait trajectory from one subject or a normative gait trajectory was tested for proof-of-concept of mechanism synthesis [19–24]. This tremendously limits generalizability due to data bias and lack of information on other factors. The comparative examination in this study, utilizing low-bias cross-validation, provides a trustworthy, data-independent result. Also, extended analysis using simulated gait patterns provides insight regarding the effect of height and gait speed on kinematic accuracy.

The guiding philosophy behind the 1 DOF gait trainer is that inducing proprioceptive input as close as possible to natural gait will be most beneficial for recovery, and there is some evidence to support this hypothesis [45,46]. Thus, training a natural gait motion along with inducing ground contact are crucial elements of the design. This study assumes that accurately assisting an ankle position in the sagittal plane could guarantee a natural proprioceptive input. However, it should be noted that a proper proprioceptive input would be further facilitated by controlling ankle orientation. The Lokomat and the gait trainers described here, with the exception of an additional cam design for the six-bar mechanism [22], ignore ankle orientation. It is assumed that dorsiflexion is provided by elastic supports or through an ankle-foot orthosis. Future work should address whether the increased complexity of a controlled orientation of the ankle is justified.

This work is limited in its conclusions because it only compares three candidate mechanism configurations. There exist other possibilities, such as inversions of six-bar [43,47] and eight-bar [48,49] or more complex (e.g., ten-bar [23]) mechanisms that could have been considered for gait trainers, orthoses, and walking robots. It is possible that other six-bar and eight-bar configurations may perform more effectively compared to the examined Stephenson III six-bar and Jansen mechanism. We limited our scope to only Stephenson III and Jansen because they have been offered recently as candidate robotic gait trainers [22,25–27]. We also did not examine designs with sliders or cams [22,24,50]. We avoided these design elements because they are not easily adjusted to fit an individual's gait trajectory. While we introduced the two-objective optimization for a comprehensive benchmark, researchers can differently configure the objective function based on J_1 and J_2 to obtain the linkage design appropriate for their specific operating scenario. Thus, while different solutions may be obtained by reducing cost functions to a single objective, we did not find any changes in the relationships between mechanisms in these conditions. There exist advanced methodologies that can draw an exact solution passing through precision points [51,52]. Although we employed a numerical approach in order to modulate cost function to fit for the targeted outcomes of comparison, such precise synthesis method should be considered to improve motion accuracy in future development. Another limitation is that the size of the mechanism and potential mechanical problems were not taken into consideration in this study. A compact device is preferable in a clinical environment and less problematic in practical application. For instance, the challenges faced with uncertainties arising from the manufacturing, assembly, sensors, control, and also numerical round-off errors would be severe in an eight-bar mechanism design. Future development should consider size and other practical issues with a novel approach taking any uncertainties into the mechanism synthesis [53]. Finally, our conclusions are limited to kinematic accuracy and mechanical advantage; considerations such as dynamics and controller performance are out of the scope of this work.

6. Conclusion

Recent research has offered numerous single DOF robotic gait trainer designs, but there is no systematic evidence comparing the performance of these designs. Our work focuses on the kinematic tracking error of three candidates, four-bar, six-bar, and eight-bar mechanism configurations. We observed that at constant crank velocity, such as controlled by a treadmill, the eight-bar mechanism has the best kinematic tracking, but all perform similarly if the crank velocity is well-controlled by an independent actuator. This work offers a quantitative approach to determining the relative performance between training mechanisms. This information will help determine cost-effective training solutions for rehabilitation clinics and possibly even home use.

Declaration of Competing Interest

The authors declare that they have no known competing financial interests or personal relationships that could have appeared to influence the work reported in this paper.

Supplementary materials

Supplementary material associated with this article can be found, in the online version, at doi:10.1016/j.mechmachtheory.2021.104258.

References

[1] H.S. Jørgensen, H. Nakayama, H.O. Raaschou, T.S. Olsen, Recovery of walking function in stroke patients: the copenhagen stroke study, Arch. Phys. Med. Rehabil. 76 (1) (1995) 27–32.
[2] M. Wyndaele, J.J. Wyndaele, Incidence, prevalence and epidemiology of spinal cord injury: what learns a worldwide literature survey? Spinal Cord 44 (9) (2006) 523–529.
[3] S. Sulzer James, E. Gordon Keith, Y. Dhaher Yasin, A. Peshkin Michael, L. Patton James, Preswing knee flexion assistance is coupled with hip abduction in people with stiff-knee gait after stroke, Stroke 41 (8) (2010) 1709–1714.
[4] T. Akbas, K. Kim, K. Doyle, K. Manella, R. Lee, P. Spicer, M. Knikou, J. Sulzer, Rectus Femoris Hyperreflexia Contributes to Stiff-Knee Gait after Stroke, J. NeuroEngineering Rehabil. 17 (1) (2020) 117.
[5] T. Akbas, S. Prajapati, D. Ziemnicki, P. Tamma, S. Gross, J. Sulzer, Hip circumduction is not a compensation for reduced knee flexion angle during gait, J. Biomech. 87 (2019) 150–156.
[6] T. Akbas, R.R. Neptune, J. Sulzer, Neuromusculoskeletal simulation reveals abnormal rectus femoris-gluteus medius coupling in post-stroke gait, Front. Neurol. (2019) 10.
[7] G. Kwakkel, B. Kollen, J. Twisk, Impact of time on improvement of outcome after stroke, Stroke 37 (9) (2006) 2348–2353.
[8] M. Camicia, H. Wang, M. Divita, J. Mix, P. Niewczyk, Length of stay at inpatient rehabilitation facility and stroke patient outcomes, Rehabil. Nurs. 41 (2) (2016) 78–90.
[9] R.P. Van Peppen, G. Kwakkel, S. Wood-Dauphinee, H.J. Hendriks, P.J. Van der Wees, J. Dekker, The impact of physical therapy on functional outcomes after stroke: what's the evidence? Clin. Rehabil. 18 (8) (2004) 833–862.
[10] S.C. Cramer, J.D. Riley, Neuroplasticity and brain repair after stroke, Curr. Opin. Neurol. 21 (1) (2008) 76–82.
[11] G. Colombo, M. Joerg, R. Schreier, V. Dietz, Treadmill training of paraplegic patients using a robotic orthosis, J. Rehabil. Res. Dev. 37 (6) (2000) 693–700.
[12] R. Riener, Technology of the robotic gait orthosis lokomat, in: Neurorehabilitation Technology, Second Edition, Springer International Publishing, 2016, pp. 395–407.
[13] J. Mehrholz, S. Thomas, C. Werner, J. Kugler, M. Pohl, B. Elsner, Electromechanical-assisted training for walking after stroke, Cochrane Database Syst. Rev. 2017 (5) (2017).
[14] K.Y. Nam, H.J. Kim, B.S. Kwon, J.W. Park, H.J. Lee, A. Yoo, Robot-Assisted Gait Training (Lokomat) improves walking function and activity in people with spinal cord injury: a systematic review, J. Neuro. Eng. Rehabil. 14 (1) (2017) 24.
[15] S. Hesse, D. Uhlenbrock, A mechanized gait trainer for restoration of gait, J. Rehabil. Res. Dev. 37 (6) (2000) 701–708.
[16] S. Hesse, C. Werner, D. Uhlenbrock, S.V. Frankenberg, A. Bardeleben, B. Brandl-Hesse, An electromechanical gait trainer for restoration of gait in hemiparetic stroke patients: preliminary results, Neurorehabil. Neural Repair 15 (1) (2001) 39–50.
[17] N. Smania, C. Geroin, N. Valè, M. Gandolfi, The End-Effector Device for Gait Rehabilitation, in: G. Sandrini, V. Homberg, L. Saltuari, N. Smania, A. Pedrocchi (Eds.), Advanced Technologies for the Rehabilitation of Gait and Balance Disorders, Springer International Publishing, Cham, 2018, pp. 267–283.
[18] V. Dietz, Proprioception and locomotor disorders, Nat. Rev. Neurosci. 3 (10) (2002) 781–790.
[19] Z. Ji, Y. Manna, Synthesis of a pattern generation mechanism for gait rehabilitation, J. Med. Devices Trans. ASME 2 (3) (2008).
[20] K. Kora, J. Stinear, A. McDaid, Design, analysis, and optimization of an acute stroke gait rehabilitation device, J. Med. Devices Trans. ASME 11 (1) (2017).
[21] B.Y. Tsuge, M.M. Plecnik, J.M. McCarthy, Homotopy directed optimization to design a six-bar linkage for a lower limb with a natural ankle trajectory, J. Mech. Robot. 8 (6) (2016) 1–7.
[22] B.Y. Tsuge, J.M. McCarthy, An adjustable single degree-of-freedom system to guide natural walking movement for rehabilitation, J. Med. Devices Trans. ASME 10 (4) (2016).
[23] B.Y. Tsuge, J.M. McCarthy, Synthesis of a 10-bar linkage to guide the gait cycle of the human leg, Proceedings of the ASME Design Engineering Technical Conference, American Society of Mechanical Engineers, 2015.
[24] Y. Shao, Z. Xiang, H. Liu, L. Li, Conceptual design and dimensional synthesis of cam-linkage mechanisms for gait rehabilitation, Mech. Mach. Theory 104 (2016) 31–42.
[21] S.Y. Shin, A.D. Deshpande, J. Sulzer, Design of a single degree-of-freedom, adaptable electromechanical gait trainer for people with neurological injury, J. Mech. Robot. 10 (4) (2018) 044503.
[26] M.R. Sabaapour, H. Lee, M.R. Afzal, A. Eizad, J. Yoon, Development of a novel gait rehabilitation device with hip interaction and a single DOF mechanism, in: 2019 International Conference on Robotics and Automation (ICRA), 2019, pp. 1492–1498.
[27] M.R. Haghjoo, H. Lee, M.R. Afzal, A. Eizad, J. Yoon, Mech-walker: a novel single-DOF linkage device with movable-frame for gait rehabilitation, IEEEASME Trans. Mechatron. (2020) 1 –1.
[28] Y. Yun, H.C. Kim, S.Y. Shin, J. Lee, A.D. Deshpande, C. Kim, Statistical method for prediction of gait kinematics with gaussian process regression, J. Biomech. 47 (1) (2014) 186–192.
[29] B. Koopman, E.H.F. van Asseldonk, H. Van der Kooij, Speed-dependent reference joint trajectory generation for robotic gait support, J. Biomech. 47 (6) (2014) 1447–1458.

[30] D.A. Cunningham, P.A. Rechnitzer, M.E. Pearce, A.P. Donner, Determinants of self-selected walking pace across ages 19 to 66, J. Gerontol. 37 (5) (1982) 560–564.
[31] S.Y. Shin, J. Sulzer, An online transition of speed-dependent reference joint trajectories for robotic gait training, in: 2019 IEEE 16th International Conference on Rehabilitation Robotics (ICORR), 2019, pp. 983–987.
[32] R. Norton, Design of Machinery: An Introduction to the Synthesis and Analysis of Mechanisms and Machines, McGraw-Hill Education, New York, 2004.
[33] I. Ullah, S. Kota, Optimal synthesis of mechanisms for path generation using fourier descriptors and global search methods, J. Mech. Des. 119 (4) (1997) 504–510.
[34] J. Yang, Z. Li, A novel contour error estimation for position loop-based cross-coupled control, IEEEASME Trans. Mechatron. 16 (4) (2010) 643–655.
[35] Y. Haimes, On a Bicriterion formulation of the problems of integrated system identification and system optimization, IEEE Trans. Syst. Man Cybern. 1 (3) (1971) 296–297.
[36] M. Laumanns, L. Thiele, E. ZitzlerJ. Branke, K. Deb, K. Miettinen, R.E. Steuer (Eds.), An adaptive scheme to generate the pareto front based on the epsilon-constraint method," *Practical Approaches to Multi-Objective Optimization*, Internationales Begegnungs- und Forschungszentrum für Informatik (IBFI), Schloss Dagstuhl (2005).
[37] M.J.D. Powell, Variable metric methods for constrained optimization, in: Mathematical Programming The State of the Art, Springer, Berlin Heidelberg, 1983, pp. 288–311.
[38] M. Stone, Cross-validatory choice and assessment of statistical predictions, J. R. Stat. Soc. Ser. B Methodol. 36 (2) (1974) 111–133.
[39] T. Hastie, R. Tibshirani, J. Friedman, The Elements of Statistical Learning: Data Mining, Inference, and Prediction, Springer Science & Business Media, 2009.
[40] Winter, D. A., 2009, *Biomechanics and Motor Control of Human Movement: Fourth Edition*.
[41] C.E. McCulloch, J.M. Neuhaus, Generalized linear mixed models, Encyclopedia of Biostatistics, American Cancer Society, 2005.
[42] S. Freivogel, J. Mehrholz, T. Husak-Sotomayor, D. Schmalohr, Gait training with the newly developed 'LokoHelp'-system is feasible for non-ambulatory patients after stroke, spinal cord and Brain injury. a feasibility study, Brain Inj 22 (7–8) (2008) 625–632.
[43] F.C. Wang, C.H. Yu, T.Y. Chou, N.C. Chang, Design and control of an active gait trainer, IEEE Int. Symp. Ind. Electron. (2009) 1779–1784.
[44] C.A. Fukuchi, R.K. Fukuchi, M. Duarte, Effects of walking speed on gait biomechanics in healthy participants: a systematic review and meta-analysis, Syst. Rev. 8 (1) (2019).
[45] V. Dietz, G. Colombo, L. Jensen, Locomotor activity in spinal man, The Lancet 344 (8932) (1994) 1260–1263.
[46] V. Dietz, Proprioception and locomotor disorders, Nat. Rev. Neurosci. 3 (10) (2002) 781–790.
[47] S. Ghosh, N. Robson, J.M. McCarthy, Kinematic design and evaluation of a six-bar knee-ankle-foot orthosis, J. Eng. Sci. Med. Diagn. Ther. 3 (2) (2020).
[48] J. McKendry, B. Brown, E.R. Westervelt, J.P. Schmiedeler, Kinematic design and dynamic analysis of a planar biped robot mechanically coordinated by a single degree of freedom, in: Proceedings - IEEE International Conference on Robotics and Automation, 2007, pp. 1875–1880.
[49] O. Al-Araidah, W. Batayneh, T. Darabseh, S.M. BaniHani, Conceptual design of a single DOF human-like eight-bar leg mechanism, Jordan J. Mech. Ind. Eng. 5 (4) (2011) 285–289.
[50] P. Zhao, L. Zhu, B. Zi, X. Li, Design of Planar 1-DOF cam-linkages for lower-limb rehabilitation via kinematic-mapping motion synthesis framework, J. Mech. Robot. 11 (4) (2019).
[51] S. Bai, Z. Li, R. Li, Exact synthesis and input–output analysis of 1-Dof PlanarLinkages for Visiting 10 Poses, Mech. Mach. Theory 143 (2020) 103625.
[52] X. Li, S. Wei, Q. Liao, Y. Zhang, A novel analytical method for four-bar path generation synthesis based on fourier series, Mech. Mach. Theory 144 (2020) 103671.
[53] J.K. Pickard, J.A. Carretero, J.-P. Merlet, Appropriate synthesis of the four-bar linkage, Mech. Mach. Theory 153 (2020) 103965.